POAC'25
St. John's, Newfoundland and Labrador, Canada

Proceedings of the 28th International Conference on Port and Ocean Engineering under Arctic Conditions
Jul 13-17, 2025
St. John's, Newfoundland and Labrador
Canada

Evaluation Method for the Validity of Pre-sawn Level Ice Test Using Image Analysis

Keisuke Anzai[1], Shigeya Mizuno[1], Yutaka Yamauchi[1]
[1] Japan Marine United Corporation, Tsu, Japan

ABSTRACT

Ice resistance is a crucial factor in the propulsion performance of icebreakers. In ice tank tests, the total ice resistance is divided into four components based on the results of resistance tests in open water, intact level ice, and pre-sawn level ice conditions. These components are used to correct test condition errors or validate numerical simulations. To accurately divide the total ice resistance, the cutting pattern of the pre-sawn level ice must be set to replicate the flow of broken ice pieces in the intact level ice condition. In this study, we evaluated the validity of the cutting pattern by comparing the flow of ice pieces in intact and pre-sawn level ice using image analysis. This image analysis method analyzed the distribution and motion of ice pieces around the hull surface using bottom-view movies of ice tank tests. The analysis results revealed differences in the flow of ice pieces between the tests in intact and pre-sawn level ice. In the pre-sawn level ice, the ice-covered area was smaller, and ice pieces were easily pushed to the sides compared to the intact level ice. Therefore, we considered that the cutting pattern used for this study was not able to replicate the resistance in level ice conditions. We consider that the image analysis method can help to set more suitable cutting patterns of pre-sawn ice tests.

KEY WORDS: Icebreaker; Pre-sawn level ice; Ice tank test; Image analysis.

INTRODUCTION

Ice resistance is one of the most basic and crucial factors in the propulsion performance of icebreakers. From the procedure of the resistance tests in ice of International Towing Tank Conference (ITTC, 2024), the total resistance in ice R_{IT} can be divided into four resistance components: resistance due to breaking the ice R_{br}, resistance due to clearing the ice R_c, resistance due to buoyancy/static clearing the ice R_b, and water resistance in ice conditions R_{IW} as shown in Equation (1).

$$R_{IT} = R_{br} + R_c + R_b + R_{IW} \quad (1)$$

In ice tank tests, the total ice resistance is divided based on the results of resistance tests in open water, intact and pre-sawn level ice conditions. Here, the pre-sawn level ice is the ice that has been pre-cut to approximate the ice breaking pattern at the bow. In this paper, the intact level ice is referred to as "level ice", and the pre-sawn level ice is referred to as "pre-sawn ice".

R_{IT} is measured in the level ice condition, R_{IW} is measured in the open water condition, and $R_c + R_b + R_{IW}$ is measured in the pre-sawn ice condition. Thus, R_{br} and $R_c + R_b$ are calculated from the difference in each result. In addition, by conducting a pre-sawn ice test at very low speed, the measured force is only R_b because it is independent of the velocity. Therefore, R_c is calculated by subtracting R_b from $R_c + R_b$.

These resistance components are used to correct test condition errors such as ice thickness, ship velocity, and hull surface friction. Moreover, numerical estimation methods for estimating ice resistance (Anzai, et al., 2021; Ionov, 1988; Lindqvist, 1989; Park, et al., 2015) calculated with dividing ice resistance into some resistance components as shown in Equation (1). Therefore, these resistance components can also be used for validating numerical estimation methods. In addition, Huang, et al. (2022) and Seo and Wang (2021) used results of pre-sawn ice tests to validate simulations of ice pieces flow using the CFD-DEM coupling method.

In the pre-sawn ice test, the cutting pattern of the ice must be set to replicate the flow of ice pieces in the level ice condition and prevent the ice pieces from additional breaking in order to divide the total ice resistance accurately. In this study, we evaluated the validity of the cutting pattern by comparing the flow of ice pieces between level ice and pre-sawn ice conditions.

For analyzing the flow of ice pieces, van der Werff, et al. (2015) used an underwater camera in pre-sawn ice tests using artificial ice. Myland (2019) analyzed bottom-view images to calculate size and number of broken ice pieces in level ice tests. In this study, our developed image analysis method (Anzai, et al., 2024) was used for analyzing the flow of ice pieces. This method analyzes distribution and movement of ice pieces around a hull surface using bottom-view movie.

ICE TANK TEST

Resistance tests in level ice and pre-sawn ice conditions were held at the Japan Marine United Ice Model Basin (JMU-IMB). The principal particulars of the model ship and the test conditions are shown in Table 1 and 2. Here, the target ice thickness was 1.5 m, and the target flexural strength of the ice was 500 kPa in full scale.

The cutting pattern of the pre-sawn ice test is shown in Figure 1. The channel width was wider than the example of ITTC (ITTC, 2024). This cutting pattern was decided based on the ice breaking pattern at the bow in the level ice tests. Moreover, we took 30 mm gaps at both edge of the channel. They were made to prevent breaking ice pieces when they rotate around the water surface.

IMAGE ANALYSIS METHOD

We analyzed the distribution and motion of ice pieces around the hull surface using image analysis. This analysis method uses bottom-view movie and considers the positional relationship between the camera and the model ship. It was developed using OpenCV.

Table 1. Principal particulars of the model ship

	Model scale	Full scale
Waterline length: L_{wl}(m)	4.7015	126.0
Waterline breadth: B_{wl}(m)	1.0075	27.0
Design draught: d(m)	0.3433	9.2
Dynamic friction coefficient between hull and ice	0.07	0.07
Scale	1/26.8	-

Table 2. Test conditions

Case	Ice type	h_i(mm)	σ_f(kPa)	E(MPa)	V_s(m/s)
LI-2kt	Level ice	59.3	15.8	6.06	0.198
LI-3kt	Level ice	55.1	18.6	7.89	0.299
LI-4kt	Level ice	57.8	17.3	11.8	0.397
PSI-2kt	Pre-sawn ice	57.4	17.8	8.82	0.199
PSI-3kt	Pre-sawn ice	55.2	18.4	7.97	0.298
PSI-4kt	Pre-sawn ice	57.1	16.6	10.9	0.398

Where h_i: Ice thickness, σ_f: Flexural strength, E: Young's modulus, V_s: Ship velocity

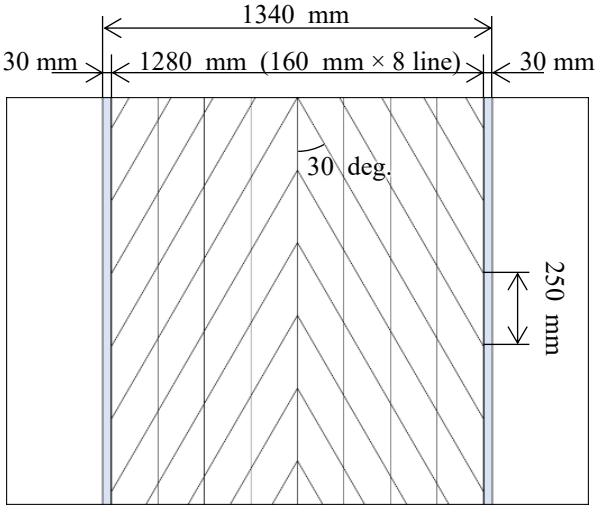

Figure 1. Ice cutting pattern of the pre-swan ice test

Matching Hull Surface to Image

The flow of ice pieces is a three-dimensional motion because broken ice pieces generally move along the hull surface. However, video images are two-dimensional and does not contain information about depth. This method estimated the three-dimensional motion from two-dimensional video images by matching the hull surface coordinates with the captured images. The target hull form was represented by the hull surface panels (Figure 2). To match the hull

surface positions with the captured image, each panel was projected onto the image reflecting the positional relationship between the camera and the model ship and the internal parameters of the camera.

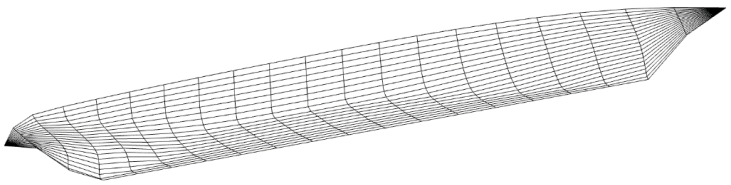

Figure 2. Hull surface panels

Analysis Method of the Distribution of Ice Pieces

The distribution of ice pieces on the hull surface was analyzed as the ice-covered ratio on each hull surface panel. Here, the ice-covered ratio means the ratio of the ice-covered area to the hull surface panel area. The analysis procedure is outlined below.

1) Extraction of ice pieces

   Ice pieces were extracted using the Otsu's threshold method (Otsu, 1979) based on the green component extracted from the RGB color image (Figure 3). The reason we used the green component is that we used the red-colored model ship. The pixels of the hull surface could be ignored by picking up the green component.

2) Projecting the hull surface panels and projective transformation

   The hull surface panels were projected onto the binary image analyzed in the above step. The correspondence between each panel and the binary image was determined (Figure 3).

   When the panel is tilted towards the camera, it causes errors for analyzing panel and ice-covered area. Therefore, images viewed from the normal direction of each panel were generated with projective transformation from the binary image.

3) Calculating the ice-covered ratio C_{ice}

   Panel area A_{pnl} and ice-covered area A_{ice} were analyzed from the generated images. The ice-covered ratio was calculated by Equation (2).

$$C_{ice} = A_{ice}/A_{pnl} \tag{2}$$

4) Calculating the time average of ice-covered ratio

   The ice-covered ratio was analyzed in each video frame, and we calculated the time average of it on each panel. Some panels were not visible depending on the video frame. Thus, we analyzed only the visible panels in each video frame. Therefore, the number of video frames used to calculate the time average differed for each panel.

5) Interpolating the ice-covered ratio on hidden area

   This analysis method used a bottom-view movie. Therefore, some panels (especially hull

side area) were hidden by hull bottom area in all video frames. When ice pieces flow into the bottom area, the hull side area is almost covered by ice pieces (Figure 4). Thus, the ice-covered ratio on the hidden panels were interpolated as below.

- When there are ice pieces under the hidden panel: $C_{ice} = 1$
- When there are no ice pieces under the hidden panel: $C_{ice} = 0$

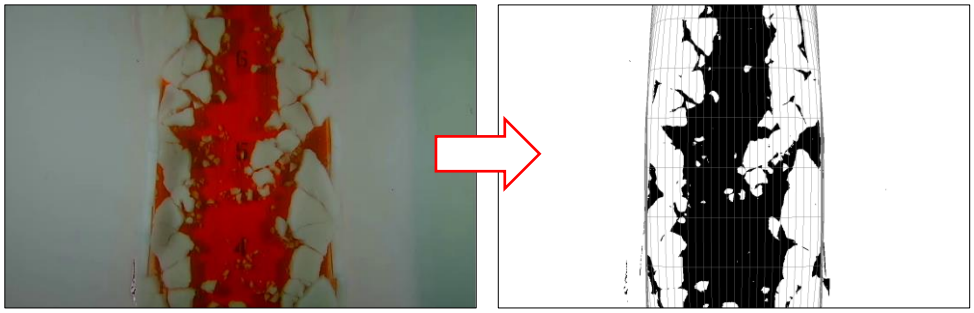

Figure 3. Result of ice pieces extraction and projection of the hull surface panels onto the image

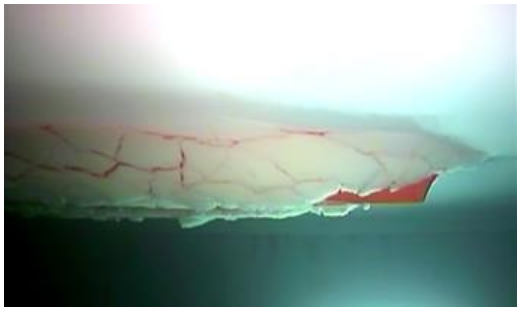

Figure 4. Distribution of broken ice pieces on a hull side area while an icebreaker goes in a level ice condition

Analysis Method of the Motion of Ice Pieces

The motion of ice pieces was analyzed three-dimensionally by estimating tracks of ice pieces. The analysis procedure is outlined below.

1) Selecting target ice pieces

   We selected target ice pieces from a frame extracted from the captured video (original color image). Figure 5 shows an example of target selection, where each blue box corresponds to each target ice piece, and the target ice pieces were manually selected. Here, the frame used for selecting targets needs to show visible gaps between ice pieces to identify clearly. In this study, we used a frame capturing the midship area of the model ship.

2) Tracking ice pieces

   The target ice pieces were tracked starting from the video frame used for their selection. They were tracked in both forward and backward directions in time as described below.

- Backward (reverse playback): Used for tracking around the fore part of the hull.

- Forward (normal playback): Used for tracking around the aft part of the hull.

Object tracking is a common problem in image analysis, and many tracking methods have been developed. In this study, we used CSR-DCF (Lukežič, et al., 2017) for tracking ice pieces. CSR-DCF stands for "Discriminative Correlation Filters with Channel and Spatial Reliability".

The DCF uses correlation filters to detect tracking targets. Fast Fourier transform is used to calculate correlation efficiently. CSR-DCF is an improvement on DCF. It incorporates the spatial reliability map to adjust the filter support to improve tracking. Moreover, the channel reliability is considered using a weighting function. CSR-DCF is a more robust method for tracking non-rectangular objects.

3) Estimating direction lines passing through the camera and the center of the target ice pieces

We estimated direction lines $l_{ci(i,f)}$ which pass through the camera and the center of each target ice piece using the tracking results and the internal camera parameters. Here, suffix i means ice pieces number (Figure 5), and suffix f means video frame number. In addition, we considered the center of each target ice piece to be the center of its corresponding rectangular tracking area.

4) Estimating three-dimensional coordinates of the target ice pieces

The three-dimensional coordinates of the target ice pieces $\boldsymbol{P}_{(i,f)} = \left(p_{x(i,f)}, p_{y(i,f)}, p_{z(i,f)}\right)$ were estimated based on $l_{ci(i,f)}$ and the positional relationship between the camera and the model ship. Since ice pieces move along the hull surface, the centers of ice pieces seem to be on the offset hull surface which is offset from the hull surface panels by half of the ice thickness (Figure 6). Therefore, we considered that $P_{(i,f)}$ is located at the intersection of $l_{ci(i,f)}$ and the offset hull surface. Figure 7 shows an overview of the plotting process.

5) Calculating the velocities of the target ice pieces

The velocities of the target ice pieces $\boldsymbol{v}_{ice(i,f)} = \left(v_{icex(i,f)}, v_{icey(i,f)}, v_{icez(i,f)}\right)$ were calculated by Equation (3). This equation is based on the moving distance between video frames and the FPS (Frames Per Second).

$$\begin{pmatrix} v_{icex(i,f)} \\ v_{icey(i,f)} \\ v_{icez(i,f)} \end{pmatrix} = FPS \begin{pmatrix} p_{x(i,f)} - p_{x(i,f-1)} \\ p_{y(i,f)} - p_{y(i,f-1)} \\ p_{z(i,f)} - p_{z(i,f-1)} \end{pmatrix} \tag{3}$$

Limitation of the image analysis method

The accuracy of the image analysis method is affected by ice thickness, the position of the hull surface panel, and its inclination (Figure 8). This method tends to overestimate the ice-covered area and misestimate the positions of ice pieces, shifting them upward and outward. However, the error of the distribution of the ice pieces seems small because the upper and hull side areas are filled with ice pieces (Figure 4). For analyzing the movement of ice pieces, we selected the target ice pieces from around the hull bottom area to minimize this error.

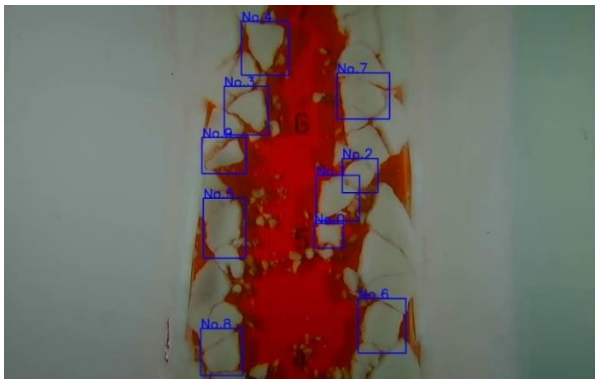

Figure 5. Target selection for tracking ice pieces (Blue boxes are selected areas)

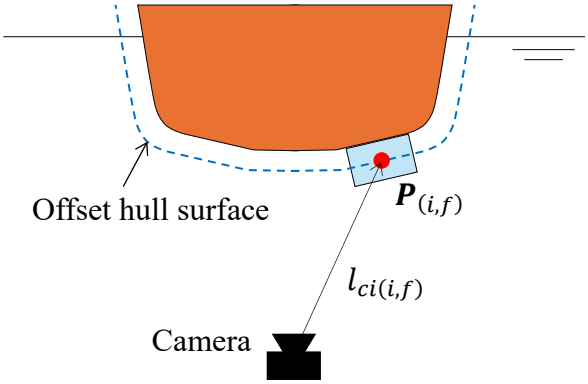

Figure 6. Outline of the estimation method for the position of an ice piece on the hull surface

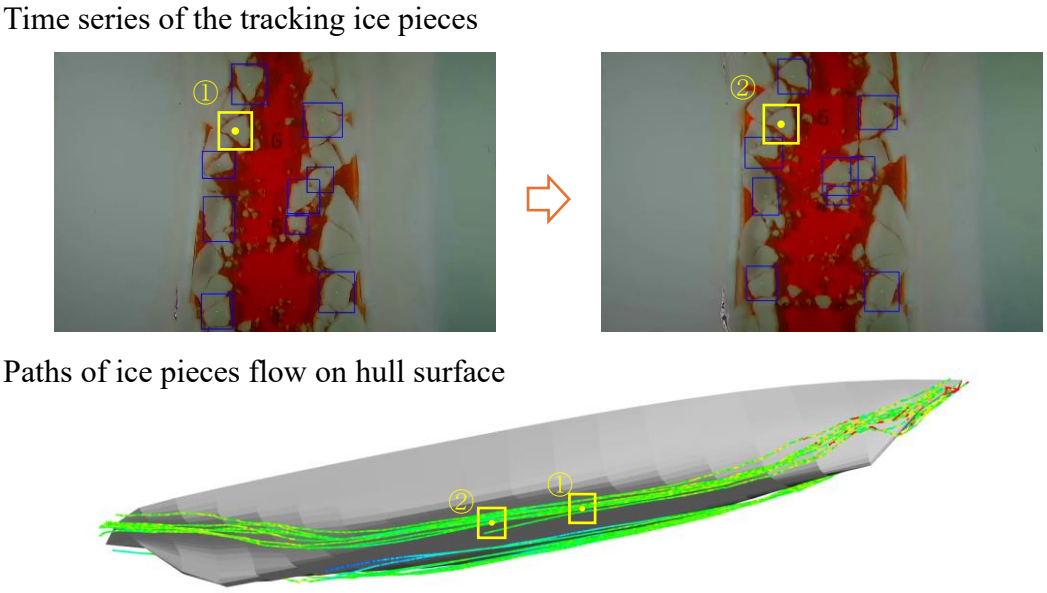

Figure 7. Overview of the plotting process. The yellow box and dot indicate the tracking area and the center of the target. Paths were plotted using the tracking results of all frames.

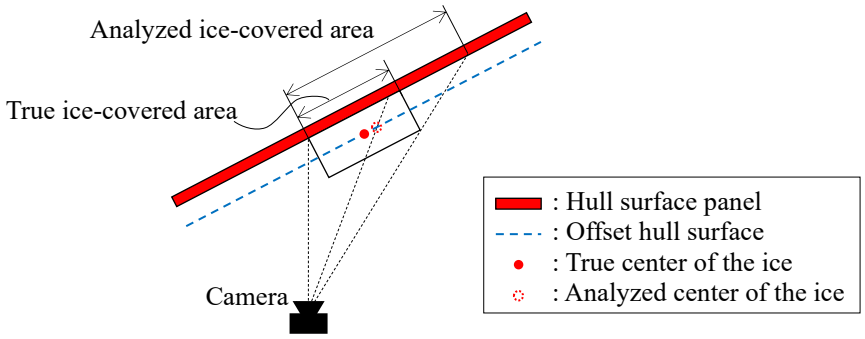

Figure 8. Analysis errors caused by ice thickness, the position of the hull surface panel, and its inclination

RESULTS

The results of the distribution of ice pieces are shown in Figure 9. Ice pieces were pushed to both side directions and they were removed from the center of the hull in all test conditions. Looking at the differences due to ice conditions, the ice-covered area in the pre-sawn ice conditions was smaller than in the level ice conditions. In addition, ice-covered area and non-ice-covered area were clearly divided in the pre-sawn ice conditions.

The results of the paths of ice pieces around the hull surface are shown in Figure 10. In the pre-sawn ice conditions, ice pieces moved more to the sides than in the level ice conditions, and ice pieces were cleared from the flat bottom area. On the other hand, some ice pieces moved into the flat bottom area in the level ice conditions. Moreover, the velocity of the ice pieces flowing into the flat bottom area decreased and they were dragged by the hull.

The initial tracking conditions are shown in Figure 11. In the level ice conditions, the size of the ice pieces varied, and there were larger gaps between the ice pieces than in the pre-sawn ice conditions.

DISCUSSION

As shown in Figure 9, in the level ice conditions, the ice pieces were more widely spread than in the pre-sawn ice conditions. Moreover, the ice pieces arrived at the flat bottom area. Therefore, the resistance due to buoyancy/static clearing the ice R_b in the level ice conditions seems to be greater than in the pre-sawn ice conditions. This is because more energy is required to push the ice pieces deeper, and the frictional resistance due to buoyancy increases when the ice pieces are located on the flat bottom area.

As shown in Figure 10, in the pre-sawn ice conditions, the ice pieces were pushed to the sides more easily than in the level ice conditions. Therefore, we consider that the resistance due to clearing the ice R_c differed between the two ice conditions. In terms of moving distance, R_c seems to be greater in the pre-sawn ice conditions because the ice pieces moved farther to the sides. However, the ice pieces flowed more smoothly in the pre-sawn ice conditions. Therefore, we cannot conclude whether R_c was greater or smaller. Comparing the results with a numerical simulation of ice pieces flow may help to analyze the difference in R_c in both ice conditions.

In the level ice conditions, the flow of the ice pieces was affected by the ship velocity. The ice pieces moved more linearly and stayed around the centerline as the ship velocity increased. Moreover, the ice pieces spread more widely. However, in the pre-sawn ice conditions, the flow of the ice pieces was not changed. This is likely because the ice pieces pushed smoothly and moved sufficiently faster than the ship velocity in the pre-sawn ice conditions. Therefore, the influence of the ship velocity seemed to be underestimated in the pre-sawn ice tests.

From these results, the flow of the ice pieces was not similar between the level ice and the pre-sawn ice conditions. The resistance components R_b and R_c seem to be different between both conditions. Thus, we conclude that the cutting pattern of the pre-sawn ice used in this test was not appropriate for dividing the ice resistance components accurately.

About the cutting pattern used for this study, we consider that channel width and gaps were too wide. In addition, one of the reasons why ice pieces did not move in the same way seems to be that they were neatly aligned in the pre-sawn conditions. This may have caused the ice pieces to move more smoothly than in the level ice conditions. Moreover, in the level ice conditions,

the size of the broken ice pieces was smaller on the inner side of the channel (Figure 11). We suggest that the width of the pre-sawn ice be made narrower on the inner side and wider on the outer side of the channel in order to replicate the broken pattern of the level ice.

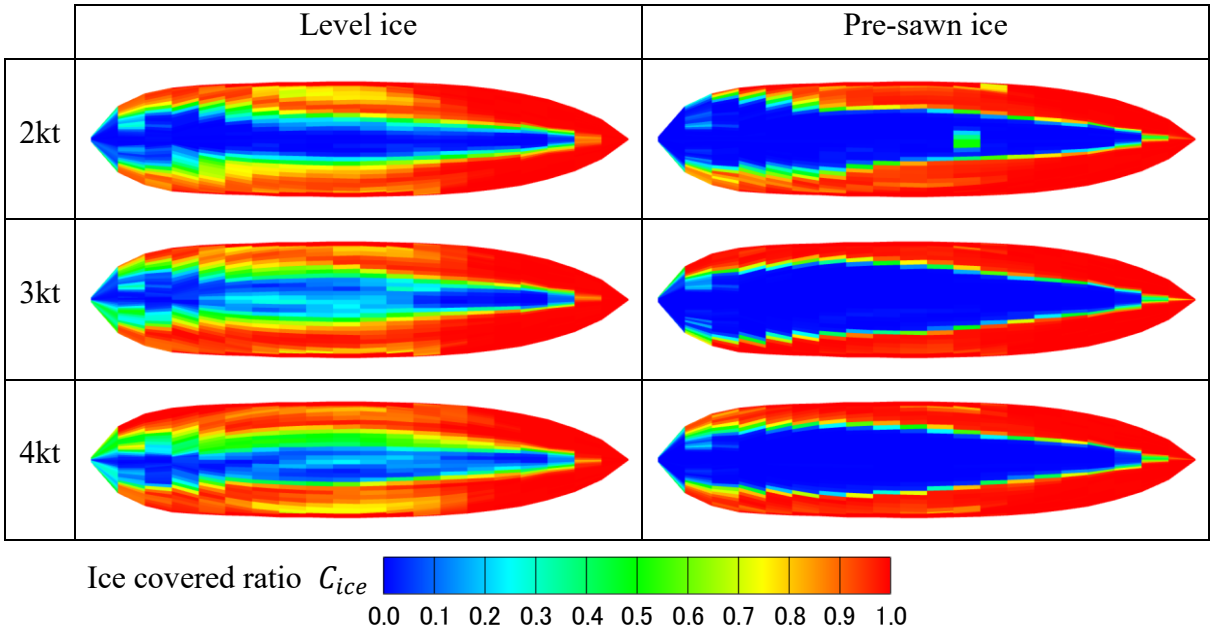

Figure 9. Distributions of ice pieces on the hull surface in the level ice and the pre-sawn ice resistance tests (bottom view). The color contour indicates the ice-covered ratio on each hull surface panel.

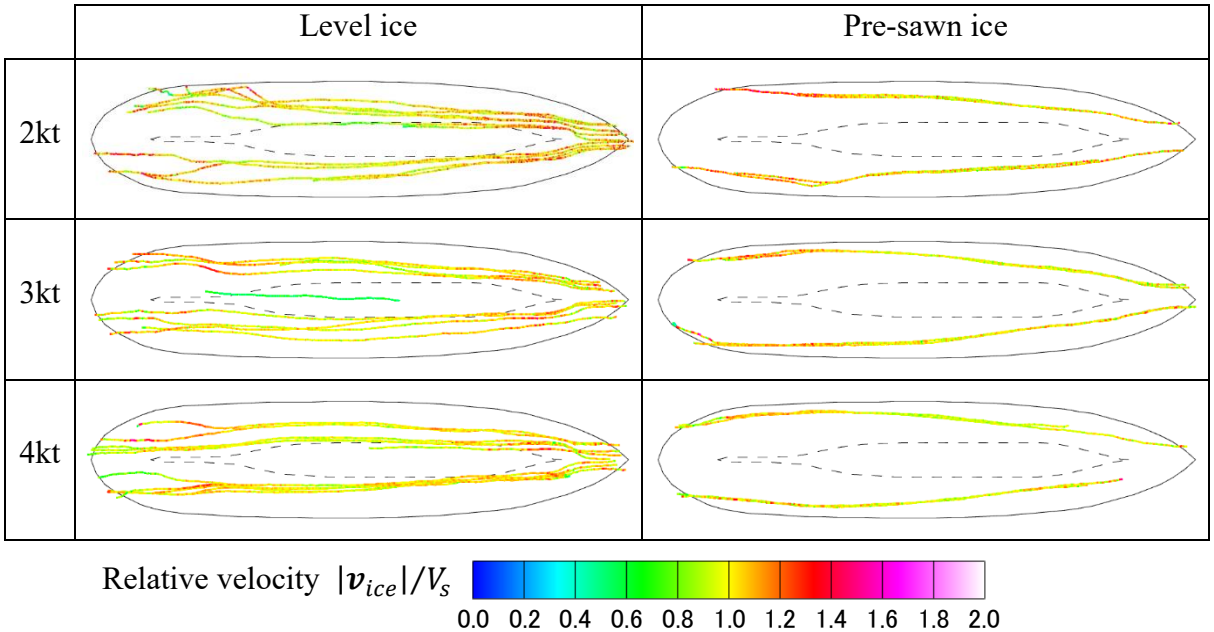

Figure 10. Paths of ice pieces around the hull surface in the level ice and the pre-sawn ice resistance tests (bottom view). The path color indicates the relative velocity (the scalar of ice pieces' velocity over the ship velocity). The outer black line shows a waterline, and the inner dashed line shows a flat bottom area.

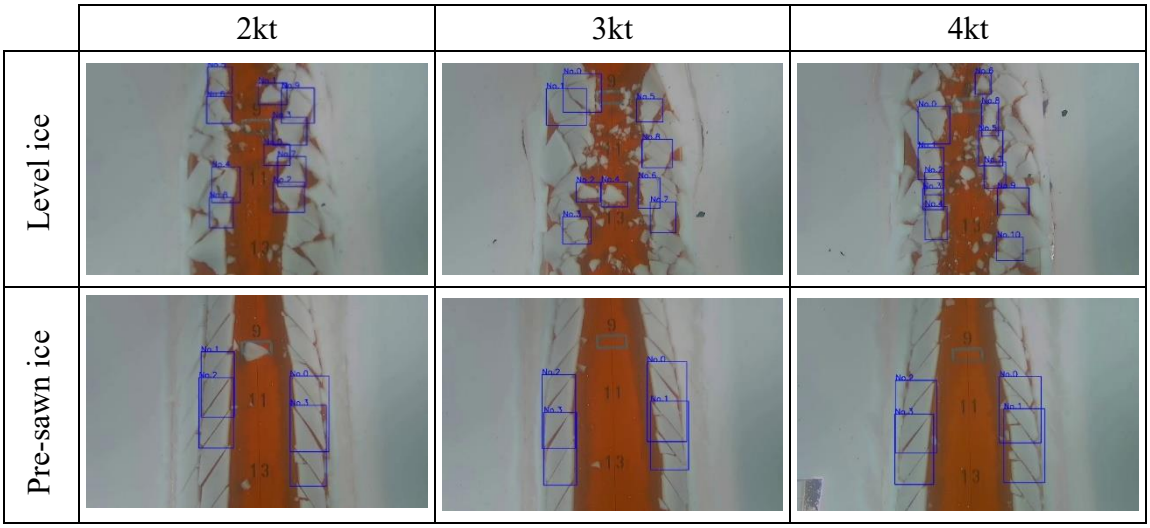

Figure 11. Initial conditions for tracking ice pieces (Blue boxes indicate selected areas)

As shown in Figure 9 and 10, the difference in the flow of the ice pieces between the level ice and the pre-sawn ice conditions was revealed using the image analysis method. We consider that the image analysis method can help to determine more suitable cutting patterns of pre-sawn ice tests.

CONCLUSIONS

The flows of ice pieces in the level ice and the pre-sawn ice conditions were analyzed and compared using the image analysis method using bottom-view movie. These tests were held at the JMU-IMB. The results are shown below.

- In the level ice tests, ice pieces spread widely and moved into the flat bottom area.
- In the pre-sawn ice tests, ice pieces were easily pushed to the sides and did not move into the flat bottom area. Moreover, ice-covered and non-ice-covered areas were clearly divided.
- Because of the differences in the flow of the ice pieces, R_b and R_c seem to have differed between the two test conditions. In addition, the influence of ship velocity seems to have been underestimated in the pre-sawn ice tests.

The difference in the flows of ice pieces between the two ice conditions was revealed using the image analysis method.

In this study, the cutting pattern of the pre-sawn ice could not replicate the flow of the ice pieces in the level ice conditions. We consider that channel width and gaps were too wide. On the other hand, we confirmed that the image analysis method can help to determine more suitable cutting patterns.

In future work, we are considering cutting patterns of pre-sawn ice to more accurately replicate the flow of ice pieces in level ice conditions with support from the image analysis method. Furthermore, we will compare the resistance and the results of image analysis. Pre-sawn ice tests at very low speed may reveal the correlation between R_b and the distributions of ice.

REFERENCES

Anzai, K., Mizuno, S., and Yamauchi, Y., 2021. *The Calculation Method of Ice Resistance in Level Ice by the Ice-Covered Hull Model*, Journal of the Japan Society of Naval Architects and Ocean Engineers, Volume 33, pp.13-24. (in Japanese)

Anzai, K., Mizuno, S., and Yamauchi, Y., 2024. *Image analysis methods for the flow of ice pieces on a hull surface in ice tank tests*, Journal of the Japan Society of Naval Architects and Ocean Engineers, Volume 39, pp.1-12. (in Japanese)

Huang, L., Li, F., Li, M., Khojasteh, D., Luo, Z., and Kujala, P., 2022. *An investigation on the speed dependence of ice resistance using an advanced CFD+DEM approach based on pre-sawn ice tests*, Ocean Engineering, Volume 264, 112530.

ITTC, 2024. *Resistance Tests in Ice*, ITTC - Recommended Procedures and Guidelines, Section 7.5-02-04-02.1.

Ionov, B. P., 1988. *ICE RESISTANCE and its components*, Arctic and Antarctic Research Institute, Leningrad. (in Russian)

Lindqvist, G., 1989. *A STRAIGHTFORWARD METHOD FOR CALCULATION OF ICE RESISTANCE OF SHIPS*, Proceedings of the 10th International Conference on Port and Ocean Engineering under Arctic Conditions, pp. 722-735.

Lukežič, A., Vojíř, T., Zajc, L. C., Matas, J., and Kristan, M., 2017. *Discriminative Correlation Filter with Channel and Spatial Reliability*, Proceedings of the IEEE Conference on Computer Vision and Pattern Recognition (CVPR), pp.6309-6318.

Myland, D. 2019. *EXPERIMENTAL AND THEORETICAL INVESTIGATIONS ON THE CHARACTERISTICS OF ICE FLOES BROKEN BY SHIPS SAILING AHEAD IN LEVEL ICE*, Proceedings of the ASME 2019 38th International Conference on Ocean, Offshore and Arctic Engineering, OMAE2019-95936.

Otsu, N., 1979. *A Threshold Selection Method from Gray-Level Histograms*, IEEE TRANSACTIONS ON SYSTREMS, MAN, AND CYBERNETICS, Volume 9, Issue 1, pp.62-66.

Park, K., Kum, M., and Kim, H., 2015. *Calculation of ice clearing resistance using normal vector of hull form and direct calculation of buoyancy force under the hull*, IJNAOE (2015), pp. 699-707.

Seo, D. C., and Wang, J., 2021. *Numerical simulation of model test in pre-sawn ice by CFD-DEM coupled method*, Proceedings of the ASME 2021 40th International Conference on Ocean, Offshore and Arctic Engineering, OMAE2021-61419.

van der Werff, S., Brouwer, J., and Hagesteijn, G., 2015. *SHIP RESISTANCE VALIDATION USING ARTIFICIAL ICE*, Proceedings of the ASME 2015 34th International Conference on Ocean, Offshore and Arctic Engineering, OMAE2015-41804.